On dependency properties of the ISIs generated by a two-compartmental neuronal model

On dependency properties of the ISIs generated by a two-compartmental neuronal model

Elisa Benedetto, Laura Sacerdote

Preprint of the paper published on *Biological Cybernetics*, February 2013,
Volume 107, Issue 1, pp 95-106.

The final publication is available at Springer via http://dx.doi.org/10.1007/s00422-012-0536-0

Biological Cybernetics manuscript No.
(will be inserted by the editor)

On dependency properties of the ISIs generated by a two compartmental neuronal model.

Elisa Benedetto · **Laura Sacerdote**

Received: date / Accepted: date

Abstract One dimensional Leaky Integrate and Fire neuronal models describe Interspike Intervals (ISIs) of a neuron as a renewal process and disregarding the neuron geometry. Many multi-compartment models account for the geometrical features of the neuron but are too complex for their mathematical tractability. Leaky Integrate and Fire two compartment models seem a good compromise between mathematical tractability and an improved realism. They indeed allow to relax the renewal hypothesis, typical of one dimensional models, without introducing too strong mathematical difficulties. Here we pursue the analysis of the two compartment model studied by Lansky and Rodriguez [16], aiming of introducing some specific mathematical results used together with simulation techniques. With the aid of these methods we investigate dependency properties of ISIs for different values of the model parameters. We show that an increase of the input increases the strength of the dependence between successive ISIs.

Keywords Two compartment neural model · ISI dependency properties

1 Introduction

The number of models for single neuron dynamics is very large and their complexity ranges from oversimplified to highly realistic biophysical models. One dimensional Leaky Integrate and Fire (LIF) model success is due to their relative simplicity jointly with their reasonable ability to reproduce neuronal input-output features. These models reproduce the membrane potential dynamics, between two consecutive neuronal

E.Benedetto, L.Sacerdote
Department of Mathematics "G.Peano", University of Torino,Via Carlo Alberto 10, 10123 Torino, Italy
Tel.: +39-0116702919
Fax.: +39-0116702878
E-mail: elisa.benedetto@unito.it
E-mail: laura.sacerdote@unito.it

firings (spikes), through one-dimensional diffusion processes $X = \{X(t); t \geq 0\}$ (cf. [7]). These stochastic processes describe the difference between the physical value of the membrane potential and the resting level. An action potential is produced when the membrane voltage X exceeds, for the first time, a voltage threshold S, often assumed to be constant. After each spike the membrane potential is reset, generally to its resting value $X(0) = x_0$ and the membrane potential evolution restarts according to the diffusion process dynamics. The interspike interval corresponds to the first passage time $T_{S,x_0} = \inf\{t \geq 0 : X(t) \geq S | X(0) = x_0\}$ of the associated stochastic process X across the boundary $S > x_0$. The assumed resetting mechanism ensures that the ISIs form a renewal process, i.e. they are independent identically distributed random variables. Then the knowledge of the renewal process corresponds to the knowledge of the distribution of T_{S,x_0}. Strong mathematical efforts have been devoted to the study of LIF models (cf. [3], [4] for a review on LIF models and [11] for a review of the mathematical tools for their study) and results have been used to analyse input-output relationships for the described neurons.

The mathematical tractability of LIF models derives from the fact that they concentrate the neuron into a single point. This choice implies not taking into account all geometrical features of the neuron.

Multi-compartment models are spatially complex models (cf. [5], [6], [8], [13], [19] and [26]). Generally they do not aim at describing the input-output properties of the neuron but focus on features related to the information processing within the neuron itself. These models are able to catch some geometrical properties of the neuron. Unfortunately the cost of this improvement is the introduction of strong mathematical difficulties related to the multivariate nature of the associated process. Since their mathematical complexity prevents the application of mathematical methods, simulation is the typical tool for their study.

Attempts to generalize single point LIF models make use of LIF paradigm in the frame of multi-compartmental models. In [2], [15], [18] and [17], two compartment LIF models are discussed. The relative simplicity of these models suggests the development of specific mathematical methods for their study.

Here, we consider the two-compartment model proposed by Bressloff (cf. [2]) and analysed by Lansky and Rodriguez in [16]. Hence we introduce two interconnected parts of the neuron: the dendritic tree and the soma. The input acts on the dendritic zone and is characterized by intensity μ and variability σ. The depolarization of the two components $(X_1(t), X_2(t))$ is described by leaky integrators with firing and reset mechanisms at the somatic zone. Hence the trigger zone is identified with the somatic one. Following [16] we introduce a firing threshold on the somatic component. The role of this threshold is the typical one of the LIF paradigm. When the somatic potential $X_2(t)$ attains the firing threshold $S > X_2(0)$ a spike is elicited. Then the value of $X_2(t)$ is reset to its resting value while the dendritic component $X_1(t)$ pursues its evolution. Both the compartments are characterized by the same leakage constant α and the junction between them depends upon a constant α_r.

The resulting model is very similar to Ornstein Uhlenbeck one-dimensional LIF model (cf. [22]). However the lack of resetting of the dendritic component destroys the renewal character of the one dimensional diffusion models. Hence the interspikes intervals determined by the two compartment model are not independent. A first study

of the ISIs of such model is proposed in [16], mainly through simulations. The aim of this paper is to pursue this analysis, through both further simulations and the aid of some analytical results. Hence we focus on dependency measures and we make use of the Kendall's τ, the correlation coefficient and the notion of copula (cf. [21]) as a possible alternative to different methods proposed in literature to analyse irregularities of ISIs (cf. [20], [23] and [24]).
This is an abstract model, as underlined in [16]. We do not claim that the use of a two dimensional process makes this model more realistic than the classical stochastic one dimensional LIF models. For example, this model assumes that the compartments are infinitely close to one another and further constrains should be introduced to make the model biologically acceptable. However we are interested on this model features because it seems one of the simplest models allowing the dependence between ISIs. This fact motivates its study, as a prototype of a model neuron of non renewal type. Our study will focus on dependency properties of ISIs, disregarding other features already studied in [16] to which we refer.

2 The model

For $t > 0$, consider a two compartment model defined by the following system of stochastic differential equations (cf. [16]):

$$\begin{cases} dX_1(t) = \{-(\alpha+\alpha_r)X_1(t) + \alpha_r X_2(t) + \mu\}\,dt + \sigma dB_t & \text{(1a)} \\ dX_2(t) = \{-(\alpha+\alpha_r)X_2(t) + \alpha_r X_1(t)\}\,dt & \text{(1b)} \end{cases}$$

with $X_1(0) = y_1$ and $X_2(0) = y_2$.
Here $X_1(t)$ and $X_2(t)$ describe the dendritic and somatic depolarization, respectively. Furthermore α and α_r are the inverse of the membrane time constant and a junctional constant, accounting for the intensity of the junction between the two components. For simplicity we assume that the membrane time constants are the same in both the compartments, however this assumption can be easily removed. Note that this model simplifies the connection between the two compartments, assuming that they are infinitely close to one the other. In absence of a firing threshold, the solution of (1a) and (1b) is a bivariate Gaussian process with mean $\mathbb{E}(\mathbf{X}(t)) = \mathbf{m}(t) = (m_1(t), m_2(t))$ given by (cf. [16]):

$$\begin{aligned} m_1(t) =& m_1(\infty) + \frac{1}{2}\left(y_1 + y_2 - \frac{\mu}{\alpha}\right)e^{-\alpha t} & \text{(2a)} \\ &+ \frac{1}{2}\left(y_1 - y_2 - \frac{\mu}{\alpha+2\alpha_r}\right)e^{-(\alpha+2\alpha_r)t} \\ m_2(t) =& m_2(\infty) + \frac{1}{2}\left(y_1 + y_2 - \frac{\mu}{\alpha}\right)e^{-\alpha t} & \text{(2b)} \\ &+ \frac{1}{2}\left(y_2 - y_1 + \frac{\mu}{\alpha+2\alpha_r}\right)e^{-(\alpha+2\alpha_r)t}. \end{aligned}$$

The depolarization $\mathbf{y} = (y_1, y_2)$ of the two components at time zero is identified with the resting potential of both the compartments when the time origin coincides with a firing time and the first component is in a stationary regime. The constants

$$m_1(\infty) = \frac{(\alpha+\alpha_r)\mu}{\alpha(\alpha+2\alpha_r)} \ , \ m_2(\infty) = \frac{\alpha_r\mu}{\alpha(\alpha+2\alpha_r)} \tag{3}$$

represent the asymptotic depolarizations. Note that the depolarization of the dendritic zone is always greater than the one of the somatic compartment. Furthermore the depolarizations of the two zones become similar when $\alpha_r \gg \alpha$. For notational simplicity we identify the resting potential with zero.
When the initial values are constant, the covariance matrix $\Gamma(t,\tau)$ has components

$$\Gamma_{11}(t,\tau) = Var(X_1(\infty)) - \tag{4}$$
$$\frac{2\alpha_r^2 k(t-\tau)^2 + \alpha\alpha_r\left(1+4k(t-\tau)+3k(t-\tau)^2\right) + \alpha^2\left(1+k(t-\tau)\right)^2}{8\alpha(\alpha+\alpha_r)(\alpha+2\alpha_r)h(t-\tau)}\sigma^2 ,$$

$$\Gamma_{22}(t,\tau) = \Gamma_{11}(t,\tau) - \frac{\sigma^2}{2(\alpha+\alpha_r)} + \frac{\sigma^2}{2(\alpha+\alpha_r)h(t-\tau)} , \tag{5}$$

$$\Gamma_{12}(t,\tau) = Cov(X_{12}(\infty)) - \frac{(\alpha+2\alpha_r)k(t-\tau)^2 - \alpha}{8\alpha(\alpha+2\alpha_r)h(t-\tau)}\sigma^2 , \tag{6}$$

$$\Gamma_{21}(t,\tau) = \Gamma_{12}(t,\tau) , \tag{7}$$

where $k(t) = e^{2\alpha_r t}$ and $h(t) = e^{2(\alpha+2\alpha_r)t}$.

Here the constants

$$Var(X_1(\infty)) = \frac{(2\alpha^2+4\alpha\alpha_r+\alpha_r^2)\sigma^2}{4\alpha(\alpha+\alpha_r)(\alpha+2\alpha_r)} \tag{8}$$

and

$$Cov(X_{12}(\infty)) = \frac{\alpha_r\sigma^2}{4\alpha(\alpha+2\alpha_r)} \tag{9}$$

denote the asymptotic dendritic variance and covariance between the two compartments, respectively.

We assume that our origin of times coincides with the epoch of a spike and we indicate with t_i the epoch of the i-th successive spike, $i \geq 1$. Then the i-th ISI, $i \geq 1$, is described by the random variable

$$T_i = \inf\{t > 0 : X_2(t) \geq S | X_2(t_{i-1}) = 0\} , \tag{10}$$

with $t_0 = 0$ and hence $T_1 = t_1$.
After each spike the somatic component is reset to its resting value while the dendritic component is not reset and continues its evolution (cf. Figure 1).

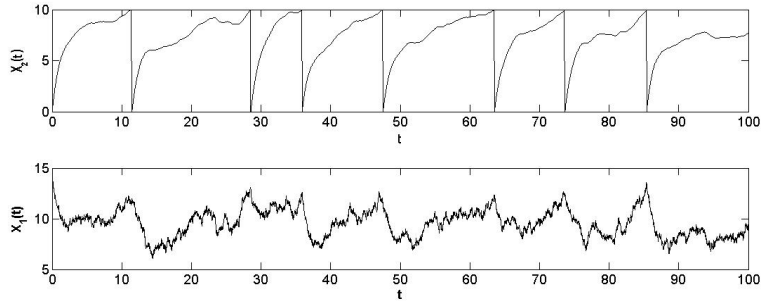

Fig. 1: Example of evolution of the dendritic (lower panel) and somatic (upper panel) components, simulated according with equations (1a), (1b). Here $\alpha = 0.05\ ms^{-1}$, $\alpha_r = 0.5\ ms^{-1}$, $\mu = 1.5\ mV$, $\sigma = 1\ mV/ms^{1/2}$, and $S = 10\ mV$.

In the following we denote with i^* the index of the spiking epoch such that the dendritic component $X_1(t)$ is statistically stationary. To estimate the value of i^* we perform Kolmogorov-Smirnov tests upon the random variables $X_1(t_i)$ and $X_1(t_{i+1})$, $i \geq i^*$, to check their identical distribution.
To study this model we separate the case of the absence of noise from the one with noise, following the classical approach of the one dimensional models.

2.1 *Absence of Noise*

When $\sigma = 0$, the time evolution of the dendritic and somatic potentials is given by equations (2a) and (2b) respectively. Hence in the subthreshold regime (i.e. $S > m_2(\infty)$) a neuron is silent. Furthermore in the suprathreshold regime (i.e. $S < m_2(\infty)$), it spikes regularly at fixed times $t_j = t_{i^*} + (j - i^*)T_{i^*}$, for $j \geq i^*$.
If the spike frequency is low the two components attain their stationary dynamics during each ISI. In fact, in this case the resetting does not influence the dendritic component evolution at the spike epochs. Then we have $m_1(t_i) = m_1(\infty)$, $m_2(t_i) = S$ and $m_2\left(t_i^+\right) = 0$, for $i \geq 1$. Here t_i^+ indicates the instant immediately following the spike. In the case of supra-threshold regime and low spiking frequency with initial condition $\{m_1(0) = m_1(\infty), m_2(0) = 0\}$, each ISI T_i, $i \geq 1$, is solution of (cf. [16]):

$$S - m_2(\infty) = \left(e^{-\alpha T_i} + e^{-(\alpha+2\alpha_r)T_i}\right) \frac{S - m_2(\infty)}{2} + e^{-2(\alpha+\alpha_r)T_i} m_2(\infty). \qquad (11)$$

This equation relates the spiking times with the asymptotic depolarization of the somatic component, whenever the dendritic component attains its stationary dynamics during each ISI.
Since the dendritic potential evolution is perturbed by the resetting of the somatic component, the stationary regime is not attained during the first ISI. Therefore, in general (11) holds for any T_j, with $j \geq i^* + 1$.

2.2 *Presence of Noise*

For $\sigma > 0$, the value of the dendritic component at spiking epochs is random and its distribution depends upon the preceding dynamics of the process. Hence a dependency between ISIs and the past evolution of the neuronal depolarization appears.
When the dendritic component is stationary, approximate formulas relating ISIs and the values of the dendritic component at spike epochs can be proved. To obtain these formulas we integrate equation (1b) between two spike times, t_{i-1} and t_i, for $i \geq 2$. Note that the somatic component can not attain values larger than S on $t \in (t_{i-1}, t_i)$, $i \geq 1$. Hence we introduce the process $X_2^B(t)$, with $t \in (t_{i-1}, t_i)$, $i \geq 2$, to model the somatic depolarization. $X_2^B(t)$ sample paths coincide with those of $X_2(t)$ that have not crossed S for $t \in (t_{i-1}, t_i)$, $i \geq 1$. Then, by definition, $X_2^B(t_{i-1}^+) = 0$ and $X_2^B(t_i) = S$. In mathematics $X_2^B(t)$ is known as a Bridge process not crossing the boundary S on $t \in (t_{i-1}, t_i)$, $i \geq 1$ (cf. [12]). On $t \in (t_{i-1}, t_i)$ it is solution of

$$X_2^B(t_i) - X_2^B(t_{i-1}) = -(\alpha + \alpha_r) \int_{t_{i-1}}^{t_i} X_2^B(t)dt + \alpha_r \int_{t_{i-1}}^{t_i} X_1(t)dt\,. \tag{12}$$

In order to determine a relationship between the value of the dendritic component at t_{i-1} and the ISI T_i, we separate the analysis of (12) in the two cases of subthreshold and suprathreshold regimes.

2.2.1 Supra-threshold regime

When the input is strong, ISIs are short and $X_2^B(t)$ can be approximated by $X_2(t)$ for $t \in (t_{i-1}, t_i)$, with $X_2(t_i) = S$. Indeed, in this case, multiple crossings of the threshold on a short interval are rare and a small percentage of sample paths of $X_2(t)$ have not a corresponding one of $X_2^B(t)$. The fast spiking activity makes the ISIs dependent random variables. The dendritic component does not attain its stationary regime during each ISI and it assumes different values at spike epochs. Hence the value of the dendritic depolarization at time t_{i-1} depends upon the past dynamics of process $\{\mathbf{X}(t), t < t_{i-1}\}$. We denote with $M_{i-1} = \mathbb{E}[X_1(t_{i-1}) | \mathbf{X}(t), t < t_{i-1}]$ the expected value of the dendritic component conditioned upon the previous history of the process. Then conditioning (12) upon $\{\mathbf{X}(t), t < t_{i-1}\}$ and taking the expectation we get (cf. Appendix A.1):

$$2(S - m_2(\infty)) = \left\{ M_{i-1} - \frac{\mu}{\alpha} \right\} e^{-\alpha T_i} + \left\{ \frac{\mu}{\alpha + 2\alpha_r} - M_{i-1} \right\} e^{-(\alpha + 2\alpha_r) T_i}. \tag{13}$$

Hence the distribution of the $i-th$ ISI T_i depends from the past evolution of the process only through the conditional expectation of the dendritic component at the previous spiking epochs.
When $\alpha \to 0$ and $e^{-\alpha T_i} \approx 1$, equation (13) can be solved to get:

$$T_i \approx -\frac{1}{\alpha + 2\alpha_r} \ln \left(1 - \frac{2S}{M_{i-1} - \frac{\mu}{\alpha + 2\alpha_r}} \right) \quad i = 1, 2, \ldots \tag{14}$$

The approximated equation (14) holds when the argument of the logarithm is positive. Therefore to determine the distribution of T_i one should know the entire history of the process. However when the conditional random variables $\{M_j\}$ are identically distributed and their distribution does not depend upon the previous evolution of the process, then the interspike intervals $\{T_{j+1}\}$ become identically distributed. Indeed this happens for any $j \geq i^*$ when the ISI distribution depends only from the distribution of M_j at the previous spiking epochs, since the dendritic component is stationary. Moreover, the ISIs of a collection $(T_i, T_{i+1}, ..., T_{i+n})$ are dependent since M_i depends upon T_{i-1}. A further approximation of (14)

$$T_i \approx \frac{1}{\alpha + 2\alpha_r} \left(\frac{2S}{M_{i-1} - \frac{\mu}{\alpha+2\alpha_r}} \right) \tag{15}$$

holds when $\frac{2S}{\frac{\mu}{\alpha+2\alpha_r} - M_{i-1}}$ is small enough, i.e. for large input. Hence the mean firing frequency is approximately

$$\mathbb{E}\left(\frac{1}{T_i}\right) \approx \frac{\alpha + 2\alpha_r}{2S} \left(\mathbb{E}(M_{i-1}) - \frac{\mu}{\alpha + 2\alpha_r} \right) \tag{16}$$

and its variance is

$$Var\left(\frac{1}{T_i}\right) \approx \left(\frac{\alpha + 2\alpha_r}{2S}\right)^2 Var(M_{i-1}). \tag{17}$$

Furthermore for the correlation we get:

$$\rho\left(\frac{1}{T_i}, \frac{1}{T_{i-1}}\right) \approx \rho(M_{i-1}, M_{i-2}). \tag{18}$$

Formulas (14)-(18) are not useful for computational aims. Indeed their use requests the knowledge of the moments of the conditional random variable M_{i-1}. However they are interesting because they illustrate the relationship between the moments of the random variables T_i and M_{i-1}.

2.2.2 Sub-threshold regime

When the somatic depolarization is in the sub-threshold regime, formulas from (13) to (18) do not hold. However, in this case, the attainment of the threshold is rare and it is determined by the noise. For moderate noise intensity, interspike intervals increase and the dendritic component attains its stationary behaviour during each ISI. Hence we can postulate the identical distribution of T_{i+1}, $i \geq 1$. Furthermore in this case, during each ISI, the process forgets the initial value of the dendritic component. Hence the ISIs are approximately independent and identically distributed. The presence of the renewal property makes the features of the two compartment model similar to those of one-dimensional one. Hence our interest focuses mainly on the supra-threshold regime.

2.2.3 Distribution of T_i

When the dendritic component is stationary the ISIs are identically distributed, hence $T_i \sim T$ for any $i > i^*$. In this case we determine the ISI distribution. For this aim we introduce a bidimensional generalization of the celebrated Fortet equation for the first passage time distribution. Let

$$g(S,t|(y_1,y_2)) = \frac{\partial}{\partial t}\mathbb{P}(T < t|(y_1,y_2),\tau) \tag{19}$$

be the first passage time probability density function of the somatic component through $S > y_2$. It holds (cf. [1]):

$$f(\mathbf{x},t \mid \mathbf{y},\tau) = \tag{20}$$

$$= \int_\tau^t d\vartheta \int_{-\infty}^{+\infty} g(S,\vartheta \mid \mathbf{y},\tau)\frac{\partial}{\partial z}\mathbb{P}(X_1(T_S) \le z|T_S = \vartheta)f(\mathbf{x},t \mid (S,z),\vartheta)\,dz.$$

Here $\mathbf{y} = (y_1,y_2)$ with $y_2 = 0$, due to the resetting procedure, and $\mathbf{x} = (x_1,x_2)$ with $x_2 > S$. The transition probability density of the process $(X_1(t),X_2(t))$ originated in $\mathbf{y} = (y_1,y_2)$, $f(\mathbf{x},t \mid \mathbf{y},\tau)$, is Gaussian with mean given by (2) and (3) and covariance matrix given by (5)-(8). One can solve (20) for fixed initial values of the dendritic component y_1. Since y_1 is assumed stationary, in the sequel we choose $y_1 \approx m_2(\infty)$. An analytical solution of (20) is not available but a numerical method for its solution is proposed in [1].

2.2.4 Dependency between ISI

ISIs of the two compartment model are dependent for specific choices of the parameters. To check the presence of dependencies between successive ISIs we estimate the correlation coefficient ρ and the Kendall's τ. The latter is an index preferable to the former when we are investigating non linear dependencies between random variables (cf. [9]). The Kendall's τ between two random variables X and Y is defined as the difference between the probabilities of concordance and discordance for two independent copies (X_1,Y_1) and (X_2,Y_2) of the bivariate random variable (X,Y) (cf. [14]), that is

$$\tau = \mathbb{P}\{(X_1 - X_2)(Y_1 - Y_2) > 0\} - \mathbb{P}\{(X_1 - X_2)(Y_1 - Y_2) < 0\}. \tag{21}$$

Considering a set of n observations $\{(x_i,y_i), i = 1,\dots n\}$ of (X,Y), the couples (x_i,y_i) and (x_j,y_j) are concordant if $(x_i - x_j)(y_i - y_j) > 0$, for $i \neq j$, otherwise they are discordant. Then an estimator $\hat{\tau}$ of the Kendall's τ is

$$\hat{\tau} = \frac{(\text{number of concordant pairs}) - (\text{number of discordant pairs})}{n(n-1)/2} \tag{22}$$

where $n(n-1)/2$ is the total number of pairs.
When the parameters of the process are such that the ISIs are identically distributed but dependent, one can study the joint distribution of successive ISIs determining the

associated copula $C(u,v)$, $(u,v) \in [0,1] \times [0,1]$. In Appendix A.2 we introduce basic ideas on copulas, while we refer to [21] for a complete introduction to the topic. Here we limit ourselves to recall that the joint distribution function $F_{T_1,T_2}(t_1,t_2) = \mathbb{P}(T_1 < t_1, T_2 < t_2)$ of two random variables T_1 and T_2 with marginal distributions $F_{T_i}(t_i) = \mathbb{P}(T_i < t_i)$, $i = 1,2$, verifies

$$F_{T_1,T_2}(t_1,t_2) = C(F_{T_1}(t_1), F_{T_2}(t_2)) . \tag{23}$$

The shape of $C(u,v)$ can be determined from modelling arguments or can be argued from plots and confirmed through statistical tests. In this paper we follow this last procedure.

3 Results

To discuss features of the model we make use of the approximated formulas of the previous Section and of simulations. Here we focus on dependency properties between ISIs as the parameter values vary, while we refer to [16] for further properties. Where not differently established, the parameters values are: $S = 10\ mV$, $\alpha = 0.05\ ms^{-1}$, $\alpha_r = 0.5\ ms^{-1}$, $\sigma = 1\ mV/ms^{1/2}$, $\mu \in [1,5]\ mV$. We use simulations of 1000 sample paths.
We first perform a sensitivity analysis on the parameters α_r, σ and μ involved in the model. In this analysis we recognize that particular choices of the parameters make the ISIs dependent and identically distributed. Then we discuss the joint distribution of successive ISIs for these instances.

Role of α_r: the junctional constant determines the strength of the connections between the two compartments. When $\alpha_r = 0$, the somatic potential evolves independently from the dendritic one. Actually its dynamics becomes deterministic, because it does not receive noise from the dendritic component. For fixed α, as α_r increases, the dependency between the values of the dendritic component at the epochs of successive spikes decreases. In Table 1 we illustrate the dependence between two successive ISIs by means of the Kendall's τ and the correlation coefficient ρ. The estimated values of $\hat{\tau}$ and $\hat{\rho}$ refer to successive ISIs. With the choice of the parameters of Table 1, the ISI T_{i^*} and T_{i^*+j}, $j > 1$ are dependent ($\hat{\tau} > 0.1$) when $\alpha_r = 0.05$, otherwise the dependence disappears.

α_r	$\hat{\tau}$	$\hat{\rho}$	i^*
0.05	[0.39, 0.47]	[0.57, 0.65]	4
0.25	[0.11, 0.19]	[0.17, 0.29]	5
0.5	[0.10, 0.18]	[0.10, 0.22]	5
0.75	[0.03, 0.11]	[0.05, 0.16]	5

Table 1: Values of Kendall's $\hat{\tau}$ and correlation coefficient $\hat{\rho}$ (95% confidence intervals) between subsequent ISIs. Here $\alpha = 0.05\ ms^{-1}$, $\sigma = 1\ mV/ms^{1/2}$, $\mu = 3.5\ mV$ and $S = 10\ mV$. For these values of α_r the neuron is in the suprathreshold regime.

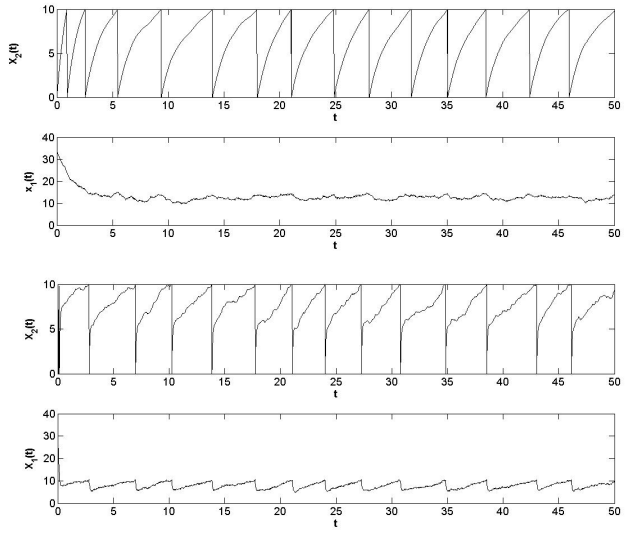

Fig. 2: Two examples of samples of the somatic (upper) and dendritic (lower) components. In panels (a) $\alpha_r = 0.5\ ms^{-1}$, while in panels (b) $\alpha_r = 10\ ms^{-1}$. Here $\alpha = 0.05$ ms^{-1}, $\mu = 3.5\ mV$ and $\sigma = 1\ mV/ms^{1/2}$.

In Figure 2 we illustrate sample paths of the dendritic and somatic components for two values of α_r. When α_r increases the somatic potential dynamics affects strongly the dendritic potential evolution. Hence, for larger values of α_r, both potentials exhibit a resetting effect at spike times and the ISIs become independent (cf. Figure 2(b)). On the contrary, in the presence of a weak coupling of the two components, the dendritic potential attains a stationary dynamics since no perturbation arrives from the somatic dynamics. Hence the bidimensional process shows renewal features only on the somatic component, generating a dependence between successive ISIs.
In Figure 3(a) we illustrate the ISIs distribution for different values of α_r. The other parameters are chosen to have identically distributed ISIs. Note that these distributions are not normal. Indeed they show slight asymmetries and the normal assumption cannot be accepted (the p-value of a normal goodness of fit test is lower than 10^{-7}).

Role of σ: The noise affects directly only the dendritic compartment. However the interconnection between the two compartments allows the input variability to influence the somatic dynamics and the distribution of ISIs. Increasing σ the dependence between successive ISIs increases (cf. Table 2). However the dependency between ISIs disappears when one considers T_{i^*} and T_{i^*+j}, $j > 1$. Furthermore, increasing σ, the ISI variability increases (cf. Table 2) and the stationary distribution of $\{M_i\}_{i \geq i^*}$ becomes more flat (figure not shown). In Figure 3(b) we illustrate some ISIs distributions for different choices of σ. Note that such distribution functions are again not normal, since they show slight asymmetries (the p-value of a normal goodness of fit test is lower than 10^{-10}). Moreover we observed that $\hat{\tau}$ captures the ISI

dependencies better than $\hat{\rho}$. This fact is related to the properties of the two indexes τ and ρ. The correlation index ρ detects linear dependencies while τ does not hypothesizes specific shapes of the dependencies.

σ	i^*	$\sigma(T_6)$	$\hat{\tau}$	$\hat{\rho}$
0.05	6	$[0.003, 0.004]$	$[0.06, 0.14]$	$[0.07, 0.19]$
1	5	$[0.33, 0.39]$	$[0.08, 0.16]$	$[0.13, 0.25]$
5	4	$[9.21, 10.98]$	$[0.09, 0.17]$	$[0, 0.11]$
10	3	$[26.93, 32.09]$	$[0.21, 0.29]$	$[0.03, 0.15]$

Table 2: Values of i^*, Kendall's $\hat{\tau}$, correlation coefficient $\hat{\rho}$ (95% confidence intervals) and sample variance $\sigma(T_6)$ of T_6 (95% confidence interval), for different noise intensities. i^* is determined using a Kolmogorov-Smirnov test to check the identical distribution of $X_1(t_i)$ and $X_1(t_{i+1})$ for $i \geq i^*$. The other parameters are $\alpha = 0.05\ ms^{-1}$, $\alpha_r = 0.5\ ms^{-1}$, $\mu = 3.5\ mV$ and $S = 10\ mV$.

Role of μ: Examples in Table 3 show an increase of the dependence between successive ISIs as the input increases. For small values of the input μ the somatic component is in the sub-threshold regime. In this case the neuron is slow and the somatic component attains its stationary regime during each ISI.

μ	i^*	$\hat{\tau}$	$\hat{\rho}$	$\mu(T_j)_{j>i^*}$	$m_2(\infty) - S$
1	1	$[-0.05, 0.03]$	$[-0.05, 0.07]$	52.401 ms	-0.48
2	2	$[-0.02, 0.06]$	$[-0.05, 0.07]$	8.7091 ms	9.05
3	4	$[0.06, 0.14]$	$[0.10, 0.22]$	4.7324 ms	18.57
4	6	$[0.16, 0.24]$	$[0.20, 0.32]$	3.2923 ms	28.09
5	8	$[0.34, 0.42]$	$[0.33, 0.44]$	2.5176 ms	37.62

Table 3: Values of i^*, Kendall's $\hat{\tau}$ and correlation coefficient $\hat{\rho}$ (95% confidence intervals) and ISI sample mean $\mu(T_j)$ for $j > i^*$ as μ varies. In the last column the values of $m_2(\infty) - S$ allow to recognize sub-threshold and supra-threshold regimes. Here $\alpha = 0.05\ ms^{-1}$, $\alpha_r = 0.5\ ms^{-1}$, $\sigma = 1\ mV/ms^{1/2}$ and $S = 10\ mV$.

Furthermore during each ISI, the process has the necessary time to forget the initial value of the dendritic component and ISIs are independent (cf. Table 3, third and fourth column). For values of $\mu < 2\ mV$, a Kolmogorov Smirnov test on the distribution of M_i confirms that these random variables are identically distributed (with a p-value of 0.29). When the input μ increases, the ISIs decrease and $X_1(t)$ does not attain its stationary regime during the first ISI. This implies that the variables M_i are not identically distributed for small values of i. However for $i \geq i^*$ the random variables M_i become identically distributed (with a p-value of 0.53). Furthermore as μ increases successive interspikes intervals, as well as successive values of the variables M_i, $i \geq 1$, become dependent. This dependence strengthens with μ (cf. Table 3). This fact can be explained considering the decrease of the ISIs as μ increases. The

process does not forget its starting point when the spikes are frequent. In particular for $\mu > 4$ we can also observed a light dependence between ISIs T_{i^*} and T_{i^*+j} with $j > 1$ (results not shown).
In Figure 3(c) we illustrate the shape of the distribution of T_j, for $j > i^*$, as μ increases. Note that such distribution functions are not normal (the p-values of all normal goodness of fit tests are lower than 10^{-6}), as observed before for other choices of the parameters.

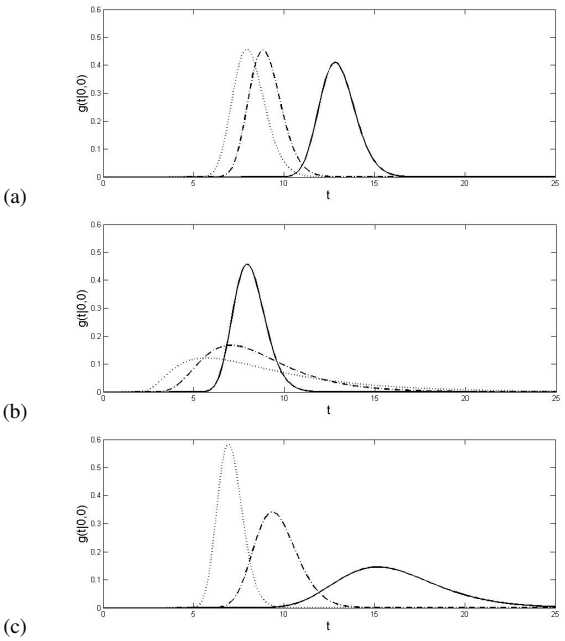

Fig. 3: Probability density functions of identically distributed ISIs through a boundary $S = 10\ mV$, computed numerically solving equation (20). In panel (a) $\alpha_r = 0.1\ ms^{-1}$ (solid), $\alpha_r = 0.3\ ms^{-1}$ (dashdot) and $\alpha_r = 0.5\ ms^{-1}$ (dotted). In panel (b) $\sigma = 1\ mV/ms^{1/2}$ (solid), $\sigma = 5\ mV/ms^{1/2}$ (dashdot) and $\sigma = 10\ mV/ms^{1/2}$ (dotted). In panel (c) $\mu = 2\ mV$ (solid), $\mu = 3\ mV$ (dashdot) and $\mu = 4\ mV$ (dotted). Furthermore $\alpha = 0.05\ ms^{-1}$, while $\alpha_r = 0.5\ ms^{-1}$ in (b) and (c), $\mu = 3.5\ mV$ in (a) and (b), $\sigma = 1\ mV/ms^{1/2}$ in (a) and (c).

Joint distribution of successive ISIs: We study the joint distribution of successive dependent and identically distributed ISIs, using some scatterplots of the associated copula for different values of μ (cf. Figure 4).
The shape of these scatterplots suggests to hypothesize the presence of a normal copula. As μ increases the scatterplot shows a stronger dependence between two subsequent ISIs, confirming the results of Table 3. A goodness of fit test confirms this conjecture, with p-values greater than 0.2. Hence the joint distribution of two

subsequent ISIs can be obtained using the Gaussian copula, with covariance matrix estimated from the data. The marginals are obtained numerically solving equation (20), but they are non Gaussian distributions (cf. Figure 3). In Figure 5 we show an example of ISI joint distribution.

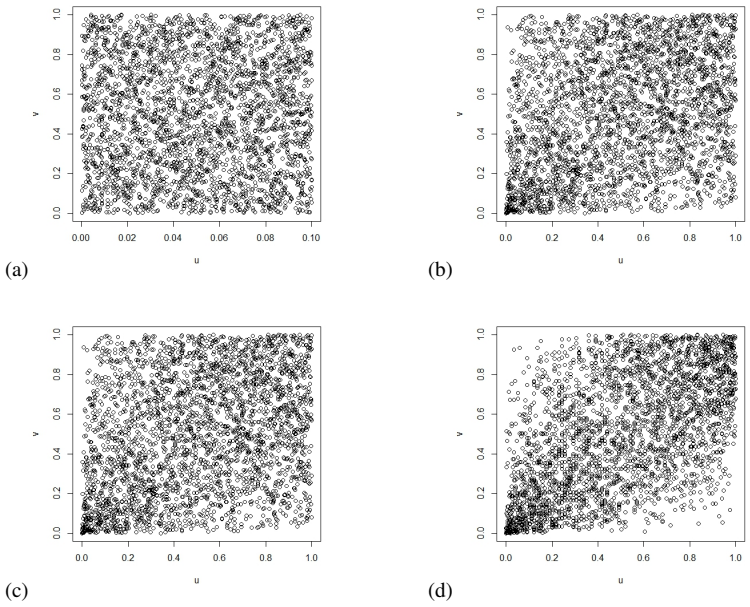

Fig. 4: Scatterplot of the copula $C(u,v)$ between T_6 and T_5 for $\mu = 2\ mV$ (a), $\mu = 3.5\ mV$ (b), $\mu = 4\ mV$ (c), $\mu = 5\ mV$ (d). Here $\alpha = 0.05\ ms^{-1}$, $\alpha_r = 0.5\ ms^{-1}$, $\sigma = 3\ mV/ms^{1/2}$ and $S = 10\ mV$.

Similar results are obtained also varying the other parameters when the successive ISIs are dependent but identically distributed. Note that the presence of a Gaussian copula between subsequent ISIs does not implies that the ISI marginals are normally distributed. In fact normal goodness of fit tests on the FPT probability density functions, shown in Figure 3, reject the Gaussian hypothesis with a p-value lower than 10^{-6}. This fact is evident in Figure 3(b), where the probability density functions with $\sigma = 5$ and $\sigma = 10$ are strongly asymmetric.

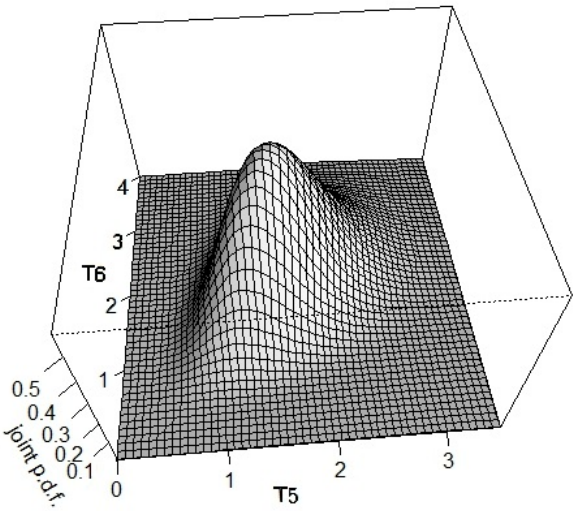

Fig. 5: Evaluation of the joint probability density of T_5 and T_6 using a normal copula with correlation coefficient of 0.4, estimated from data, and marginal distributions computed from (20). The set of the parameters is: $\alpha = 0.05\ ms^{-1}$, $\alpha_r = 0.5\ ms^{-1}$, $\mu = 4\ mV$, $\sigma = 3\ mV/ms^{1/2}$, $S = 10\ mV$.

Appendix

A.1. Proof of equation (13)

When $X_2^B(\tau) \approx X_2(\tau)$, $\tau \in (t_{i-1}, t_i)$, with t_{i-1} and t_i firing times, equation (12) becomes

$$X_2(t_i) - X_2(t_{i-1}) = -(\alpha + \alpha_r) \int_{t_{i-1}}^{t_i} X_2(t)dt + \alpha_r \int_{t_{i-1}}^{t_i} X_1(t)dt\,. \tag{24}$$

Since $X_2(t_i) = S$ and $X_2(t_{i-1}^+) = 0$, equation (24) can be rewritten as:

$$S = -(\alpha + \alpha_r) \int_{t_{i-1}}^{t_i} X_2(t)dt + \alpha_r \int_{t_{i-1}}^{t_i} X_1(t)dt\,. \tag{25}$$

Taking the expectation of each member of (25) and applying Fubini's theorem (cf.[10]), we get

$$S = -(\alpha + \alpha_r) \left[\int_{t_{i-1}}^{t_i} m_2(t)dt \right] + \alpha_r \left[\int_{t_{i-1}}^{t_i} m_1(t)dt \right]. \tag{26}$$

Now, considering the expressions (2a) and (2b) with initial condition $m_2(t_{i-1}) = 0$ and $m_1(t_{i-1}) = M_{i-1}$, we have

$$\begin{aligned} m_1(t) =& m_1(\infty) + \frac{1}{2}\left(M_{i-1} - \frac{\mu}{\alpha}\right) e^{-\alpha t} \\ &+ \frac{1}{2}\left(M_{i-1} - \frac{\mu}{\alpha + 2\alpha_r}\right) e^{-(\alpha+2\alpha_r)t} \end{aligned} \tag{27}$$

$$\begin{aligned} m_2(t) =& m_2(\infty) + \frac{1}{2}\left(M_{i-1} - \frac{\mu}{\alpha}\right) e^{-\alpha t} \\ &+ \frac{1}{2}\left(\frac{\mu}{\alpha + 2\alpha_r} - M_{i-1}\right) e^{-(\alpha+2\alpha_r)t}. \end{aligned} \tag{28}$$

Finally replacing (27) and (28) into (26) we get the following equation for the i-th ISI, $i \geq 2$

$$2(S - m_2(\infty)) = \left\{M_{i-1} - \frac{\mu}{\alpha}\right\} e^{-\alpha T_i} + \left\{\frac{\mu}{\alpha + 2\alpha_r} - M_{i-1}\right\} e^{-(\alpha+2\alpha_r)T_i}. \tag{29}$$

A.2. The bivariate copula

Copulas are mathematical objects increasingly used to describe the joint behaviour of random vectors. We introduce here only the material necessary for this paper while we refer to [21] for a detailed introduction.
A bivariate copula is the joint cumulative distribution function of a bivariate random vector (U,V) on the unit square $[0,1] \times [0,1]$ with uniform marginals:

$$C(u,v) = \mathbb{P}(U \leq u, V \leq v).$$

If $F_1(x_1)$ and $F_2(x_2)$ are the marginal distribution functions of the random variables X_1 and X_2, then

$$C(F_1(x_1), F_2(x_2)) = F(x_1, x_2) \tag{30}$$

defines a bivariate distribution function with marginals $F_1(x_1)$ and $F_2(x_2)$. Sklar (cf. [25]) established also that the converse is true. Indeed he proved that any bivariate distribution function F can be written in the form (30). Moreover if the marginal distributions are continuous, the copula representation (30) is unique.
Copulas separate the study of dependency properties from the study of marginals. On the contrary this two features are mixed in the joint distribution. Moreover copulas are invariant under increasing and continuous transformations, i.e. they are scale free. There exist different types of copulas, corresponding to different dependency structures. One example is the Gaussian copula associated to a multivariate normal distribution. It is constructed by projecting a bivariate normal distribution on the unit square $[0,1]^2$. For a given 2×2 correlation matrix Σ, the Gaussian copula is

$$C_\Sigma(u,v) = \phi_\Sigma\left(\phi^{-1}(u), \phi^{-1}(v)\right).$$

Here ϕ^{-1} denotes the inverse cumulative distribution function of a standard normal and ϕ_Σ is the joint cumulative distribution function of a bivariate normal distribution with mean vector zero and covariance matrix equal to Σ.
Note that if in (30) one uses a Gaussian copula and non Gaussian marginal distributions, the joint distribution is not a bivariate normal distribution.

Acknowledgements Work supported in part by MIUR Project PRIN-Cofin 2008.

References

1. Benedetto E., Sacerdote L. and Zucca C., A first passage problem for a bivariate diffusion process: numerical solution with an application to neuroscience., eprint arXiv:1204.5307 (2012)
2. Bressloff P.C., Dynamics of a compartmental integrate-and-fire neuron without dendritic potential reset., Physica D 80, 399-412 (1995)
3. Burkitt A.N., A review of the integrate and fire neuron model: I. Homogeneous synaptic input., Biol. Cybern. 95, 1-19 (2006).
4. Burkitt A.N. A review of the integrate and fire neuron model: II. Inhomogeneous synaptic input and network properties. Biol. Cybern. 95, 97-112 (2006).
5. Bush P.C., Sejnowski T.J., Reduced compartmental models of neocortical pyramidal cells., J. Neurosci. Method.7, Vol. 46, 159–166 (1993)
6. De Schutter E. and Bower J. M., An active membrane model of the cerebellar Purkinje cell., J. Neuropysiol. 71, 375–400 (1994)
7. Ditlevsen S., Greenwood P., The Morris-Lecar neuron model embeds a leaky integrate-and-fire model, To appear in Journal of Mathematical Biology, Preprint at arXiv.org (2011)
8. Ferguson K. A. and Campbell S.A, A two compartment model of a CA1 pyramidal neuron., Can. Appl. Math. Q. 17, No.2, 293–307 (2009)
9. Fredricks G.A. and Nelsen R.B., On the relationship between Spearman's rho and Kendall's tau for pairs of continuous random variables, Journal of Statistical Planning and Inference (2007)
10. Folland G.B., Real Analysis: modern techniques and their applications, John Wiley and Sons, Inc. (1999)
11. Giraudo M.T. and Sacerdote L., Leaky Integrate and Fire models: a review on mathematical methods and their applications, submitted for the volume Stochastic Differential Equation Models with Applications to the Insulin-Glucose System and Neuronal Modelling, submitted to Springer Lecture Notes in Mathematics Biosciences (LNMBIOS) Series, eprint arXiv:1101.5539v1 (2011).
12. Giraudo M.T., Greenwood P. and Sacerdote L., How sample paths of leaky integrate-and-fir models are influenced by the presence of a firing threshold, Neural Comput. 23, no. 7, 1743-1767 (2011)
13. Godfrey K., Compartmental Models and Their Application, Academic (1983)
14. Kendall M.G., A new measure of rank correlation, Biometrika, Vol.30 No. 1/2, 81-93 (1938)
15. Kohn A.F., Dendritic transformations on random synaptic inputs as measured from a neuron's spike train: Modeling and simulation., I.E.E.E. Trans. Biomed. Eng. 36, 44-54 (1989)
16. Lansky P. and Rodriguez R., Two-compartment stochastic model of a neuron, Physica D 132, 267–286 (1999)
17. Lansky P., Rospars J.P., Stochastic model neuron without resetting of dendritic potential. Application to the olfactory system., Biolo. Cybern. 69, 283-294 (1993)
18. Lansky P., Rospars J.P., Ornstein-Uhlenbeck model neuron revisited, Biol. Cybern. 72, 397-406 (1995)
19. Mino H., Grill W.M., Modeling of mammalian myelinated nerve with stochastic sodium ionic channels., Engineering in Medicine and Biology Society, Proceedings of the 22nd Annual International Conference of the IEEE, Vol. 2, 915 - 917 (2000)
20. Nawrot MP, Analysis and interpretation of interval and count variability in neural spike trains., Analysis of Parallel spike Trains, eds Gruen S and Rotter S, Springer, New York, 37-58 (2010)
21. Nelsen R.B., An introduction to copulas, Springer (1999)
22. Ricciardi L.M. and Sacerdote L., The Ornstein-Uhlenbeck process as a model for neuronal activity., Biol.Cyb. 35, 1-9 (1979)

23. Shinomoto S., Shima K., and Tanji J., Differences in Spiking Patterns Among Cortical Neurons, Neural Computation 15, 2823-2842 (2003)
24. Shinomoto S., Kim H., Shimokawa T., Matsuno N., Funahashi S., Shima K., Fujita I., Tamura H., Doi T., Kawano K., Inaba N., Fukushima K., Kurkin S., Kurata K., Taira M., Tsutsui K., Komatsu H., Ogawa T., Koida K., Tanji J., and Toyama K., Relating neuronal firing patterns to functional differentiation of cerebral cortex, PLoS Computational Biology, 5, e1000433 (2009)
25. Sklar A., Functions de repartition a n dimensions et leurs marges., Publ. Inst. Statist. Univ. Paris 8, 229-231 (1959)
26. Traub R. D., Wong R. K. S., Miles R. and Michelson H., A model of a CA3 hippocampal pyramidal neuron incorporating voltage-clamp data on intrinsic conductances., Journal of Neurophysiology, Vol. 66, No. 2, 635–650, (1991) Kybernetika, Vol. 9, No. 6, 449–460 (1973)